Development of the ALFRED reactor full power mode control system

Roberto Ponciroli [a, 1], Antonio Cammi [a], Alessandro Della Bona [b], Stefano Lorenzi [a], Lelio Luzzi [a, *]

[a] *Politecnico di Milano, Department of Energy, CeSNEF (Enrico Fermi Center for Nuclear Studies), via Ponzio 34/3, 20133, Milano, Italy*
[b] *Politecnico di Milano, Dipartimento di Elettronica, Informazione e Bioingegneria, via Ponzio 34/5, 20133, Milano, Italy*

Received 13 March 2014
Received in revised form
12 September 2014
Accepted 22 June 2015
Available online xxx

1. Introduction

The Lead-cooled Fast Reactor (LFR) has been selected by the Generation IV International Forum as one of the candidates for the next generation of Nuclear Power Plants (NPPs) (GIF, 2002). Advanced reactor concepts cooled by Heavy Liquid Metals (HLMs) ensure a great potential for plant simplification compared with the competing Sodium-cooled Fast Reactors (SFRs), exploiting the favourable features of using molten lead as coolant and the advantages guaranteed by the simplified plant layout (Tucek et al., 2006). Nevertheless, these features introduce additional safety concerns and design challenges, which result in severe constraints on control and controlled variables. Therefore, the procedure currently adopted in Light Water Reactors (LWRs) and SFRs, cannot be directly applied to LFRs. It is necessary to adopt a dedicated control strategy allowing for the dynamics and the constraints that characterize this reactor concept. In this paper, the design of a suitable full power mode control scheme for the Advanced Lead Fast Reactor European Demonstrator (ALFRED) (Alemberti et al., 2013), developed within the European 7th Framework Program LEADER Project (http://www.leader-fp7.eu), has been described.

As shown in Fig. 1, the definition of the control strategy for a nuclear reactor is a multi-phase and multi-disciplinary process whose final result is the controllers implementation. Because of the innovative features of the studied reactor concept, some preliminary analyses have been performed so as to properly characterize the system governing dynamics. First of all, the system stability at different operational conditions has been assessed by means of a zero-dimensional model (Bortot et al., 2013). Secondly, since for this kind of NPP no experimental data are available, it has been considered necessary to adopt a well-proven model-based

* Corresponding author.
E-*mail address:* lelio.luzzi@polimi.it (L. Luzzi).

[1] Current address: Argonne National Laboratory, Nuclear Engineering Division, 9700 South Cass Avenue, Argonne, IL 60439, United States.

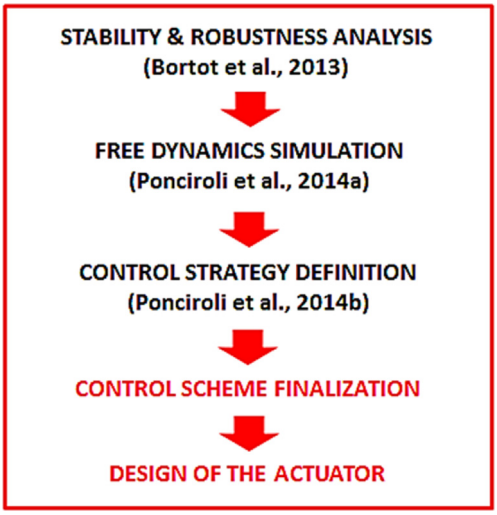

Fig. 1. Schematic view of the adopted procedure for the control system design of ALFRED. The steps previously achieved are in black (for the detailed descriptions, the reader may refer to the indicated articles). The steps developed and described in the present work are in red. (For interpretation of the references to colour in this figure legend, the reader is referred to the web version of this article.)

approach to develop the system control strategy. An object-oriented simulator (Ponciroli et al., 2014a) has been developed by employing the reliable, tested and well-documented Modelica language (Fritzson, 2004) to perform the free dynamics simulations.

As for the regulators, it has been decided to adopt a classic control scheme, such as the multiple-loop PI controller widely used in currently operated NPPs. This option represents the reference choice since it has been already licensed by the nuclear regulatory commissions for several reactors. In the perspective of developing a control strategy for a multi-variable system, it is fundamental to evaluate the influence performed by the control variables on the controlled variables in order to select the most effective couplings. To this aim, the preliminary outcomes of the simulation of the system governing dynamics have been supported by a dedicated quantitative technique such as the Relative Gain Array (RGA) method (Bristol, 1966). By adopting this approach, two possible control strategies (Ponciroli et al., 2014b) have been defined, according to the number of available control variables. The performance of the proposed strategies has been assessed through the controlled operational transients simulated by means of the developed object-oriented simulator.

The choice of a multi-loop PI control scheme, i.e., a decentralized control scheme (Skogestad and Postlethwaite, 2005), requires to prove that the different control loops do not significantly interact on each other. Preliminary indications can be obtained from the RGA outcomes, which provide an estimation of the interaction level at zero frequency for asymptotically stable processes. Nevertheless, a more accurate analysis involving the dynamic response of the system at different frequencies is advisable to evaluate the performance of the control system. In this perspective, an analytical approach based on the system transfer functions has been adopted in order to consider the interferences affecting the system controlled variables.

As last step for the finalization of the control system for ALFRED reactor, the actuator design has been considered. In the control system design, limiters on the rate of variation of the performed control actions are usually foreseen. In particular, a dedicated rate limiter should be set on the Control Rod (CR) actuator. Since the ALFRED reactor is a demonstrator of an innovative nuclear reactor concept, no experimental data concerning its dynamic behaviour are available, and the evaluation of a rate limiter for the CR reactivity can be hardly obtained. In this work, a dedicated procedure for the definition of this operational parameter based on the outcomes of the stability analysis is proposed.

The paper is organized as follows. In Section 2, a brief description of the ALFRED reactor configuration is provided, and its main features are reported. In Section 3, the definitive control scheme developed for the ALFRED reactor is defined, while in Section 4 the performance of the decentralized scheme is investigated and the effects of the mutual interactions are evaluated. In Section 5, the procedure to derive a suitable limiter on the control rod extraction speed based on the stability analysis results is described. In Section 6, two controlled operational transients are simulated, and the obtained results are discussed. Finally, the main conclusions are outlined in Section 7, while the basic features of the RGA approach adopted in the analyses are briefly given in the Appendix.

2. Reference reactor description

ALFRED is a small-size (300 MW_{th}) pool-type LFR and its primary system current configuration is depicted in Fig. 2. All the primary components (e.g., core, primary pumps and Steam Generators (SGs)) are contained in the main reactor vessel, being located in a large pool within the reactor tank. The coolant flow coming from the cold pool enters the core and, once passed through the latter, is collected in a volume (hot collector) to be distributed to eight parallel pipes and delivered to as many SGs. After leaving the SGs the coolant enters the cold pool through the cold leg and returns to the core. The ALFRED core is composed by wrapped hexagonal Fuel Assemblies (FAs) with pins arranged on a triangular lattice. The 171 FAs are subdivided into two radial zones with different plutonium fractions guaranteeing an effective power flattening, and surrounded by two rows of dummy elements serving as reflector. Two different and independent control rods systems have been foreseen, namely the CRs and the Safety Rods (SRs). Power regulation and reactivity swing compensation during the cycle are performed by the former, while the simultaneous use of both is foreseen for scram purposes, assuring the required reliability for a safe shutdown (Grasso et al., 2013). In Table 1, the major parameters employed as input data to implement the core and SG models are reported.

Each of the eight SGs incorporated in ALFRED (Fig. 3) consists in bundles of bayonet vertical tubes with external safety tube and internal insulating layer, delimited by a slave tube, which is aimed at ensuring the production of superheated dry steam since, without a proper insulation, the high temperature difference between the rising steam and the descending feedwater promotes steam condensation in the upper part of the SG. The gap between the outermost and the outer bayonet tube is filled with pressurized helium and high thermal conductivity particles to enhance the heat exchange capability and provide mechanical decoupling between the components. The feedwater from the headers flows in the slave tube and, after reversing the motion at the bottom, rises along the annulus between inner and outer tubes. On the primary side, lead flows downwards axially along the outermost tube.

3. Finalization of the ALFRED reactor control scheme

The aim of this work is the finalization and the implementation of a decentralized control scheme for the ALFRED reactor, starting from the outcomes of Ponciroli et al. (2014b) on the possible control strategies to be adopted. The choice of a decentralized control scheme has been made in virtue of its simplicity in the

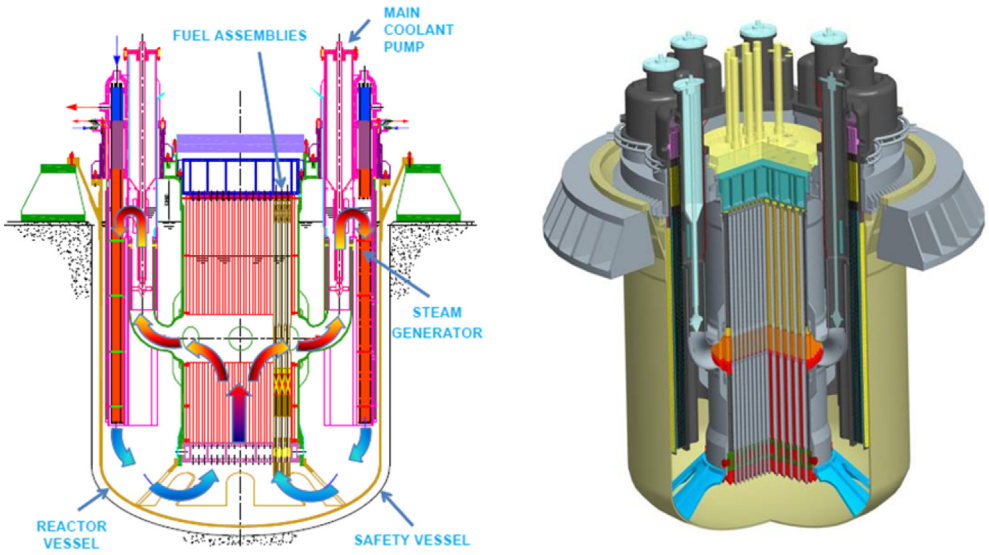

Fig. 2. ALFRED nuclear power plant layout (Alemberti et al., 2013).

Table 1
ALFRED system parameters.

Parameter	Value	Units
Thermal power	300	MW_{th}
Coolant mass flow rate	25,984	$kg \cdot s^{-1}$
Coolant SG outlet temperature	400	°C
Coolant core outlet temperature	480	°C
Pool temperature during cold shutdown	380	°C
Feedwater mass flow rate	192	$kg \cdot s^{-1}$
Water inlet temperature	335	°C
Steam outlet temperature	450	°C
SG pressure	180	bar

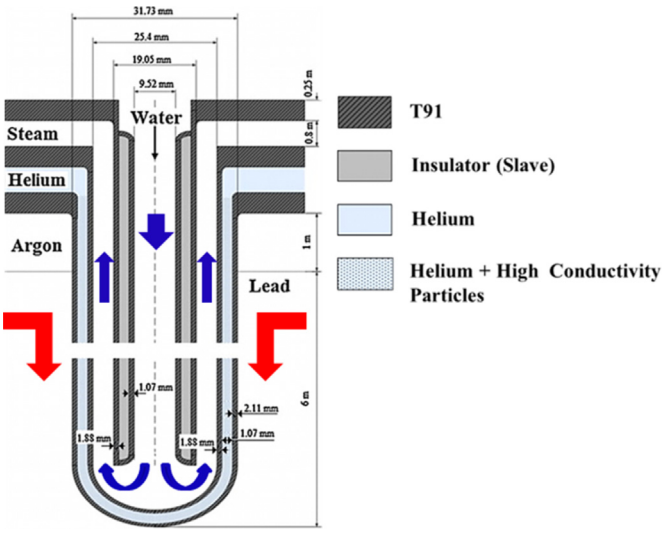

Fig. 3. ALFRED bayonet tube configuration (Alemberti et al., 2013; Damiani et al., 2013). The flow paths followed in the counter-current configuration by the lead and the water/steam are represented in red and blue, respectively. (For interpretation of the references to colour in this figure legend, the reader is referred to the web version of this article.)

implementation, which favours controllers' Operation and Maintenance (O&M), and of its robustness towards malfunctioning of the single control loops. Indeed, the multi-variable system has been regarded as if it were constituted by several SISO (Single Input Single Output) control loops, which perform a mutual interaction on each other (Levine, 1996). In the selection of the pairings between the control and the controlled variables, the preliminary analyses of Ponciroli et al. (2014b) have shown the relevance of adopting the lead mass flow rate in the primary circuit to regulate the lead temperature at the SG outlet, which has been referred to as the "cold leg" temperature. Nevertheless, the regulation of this output variable is particularly concerning since it has to be set in a narrow range because of the embrittlement of the structural materials in aggressive environment enhanced by the fast neutron irradiation (380 °C, lower limit) and the thermal creep affecting the vessel (420 °C, upper limit).

From a control-oriented perspective, the possibility of regulating the primary circuit lead mass flow rate would ensure relevant benefits to the NPP operation. First of all, observing the outcomes of the RGA matrix reported in Ponciroli et al. (2014b), the achieved pairings are more effective, and allow a better decoupling with the other outputs. Moreover, by adopting a primary circuit control variable to govern the cold leg temperature, it would be possible to adjust feedwater conditions to meet the Balance of Plant (BoP) requirements. Finally, since lead mass flow rate variations are not subject to particular constraints, the system would present a higher level of flexibility during operational transients.

However, in the design of the ALFRED reactor, it has been decided to keep fixed the lead mass flow rate to its nominal value (Alemberti et al., 2013). Indeed, one of the major efforts in the development of LFR concepts is the design of the pumps operating in the highly aggressive lead environment. In the current reactor layout, the coolant is expected to be driven by axial pumps whose restricted operating range requires a constant number of rotations per minute. In addition, maintaining the lead mass flow rate at its nominal value at reduced power levels brings benefits to the structural materials, since they operate at lower temperatures with positive effects on corrosion issues.

During the LEADER Project, the necessity of damping possible feedwater inlet temperature variations during operational transients has emerged. Otherwise, the feedwater might flow in the SG inlet at too high temperature (compromising the integrity of the centrifugal pumps or causing a thermal crisis), or at a too low temperature (leading to a local coolant solidification at the SG outlet). Therefore, a dedicated device to maintain the feedwater

inlet temperature close to its nominal value (335 °C) is envisaged. Accordingly, since both the lead mass flow rate and the feedwater inlet temperature cannot be adopted to regulate the lead temperature in the cold leg, the water mass flow rate has been employed (Fig. 4), despite the lower effectiveness shown by the RGA analysis outcomes.

In order to both design the regulators and simulate the system controlled response so as to assess the validity of the control scheme, the object-oriented model of the entire plant, whose graphical interface is represented in Fig. 5, has been adopted. Based on the Modelica language and implemented in the Dymola environment (DYNASIM software, 2006), the system simulator has been built by connecting several dedicated models (for details, see Ponciroli et al., 2014a):

- *Core model*: it is composed by three subsystems. The model *Kinetics* describes the dynamics of the neutron generation processes in the core implementing the point-wise kinetic model, with one neutron energy group and six delayed precursor groups. The model *FuelRods* is adopted to represent the thermal behaviour of the fuel pins, which are discretized in five radial regions (i.e., the cladding, the gap and three concentric zones within the pellet). The model *LeadTube* represents the coolant flowing through the core channels adopting one-dimensional mass, momentum and energy conservation equations.
- *SG Model*: as for the water side, a two-phase homogeneous model (i.e., same velocity for the liquid and vapour phases) has been adopted. On the lead side, the core component *LeadTube* is reused, describing the behaviour of a single-phase fluid.
- *Primary model*: the dynamics effects of the cold pool have been represented by employing a free-surface cylindrical tank component on which mass and energy balances are taken into account, assuming that no heat transfer occurs except through the inlet and outlet flows. In order to consider the time delay due to the transport phenomena between the core and the SG, dedicated models have been implemented. As for the integrated primary pump, an ideal mass flow rate regulator has been employed.
- *Secondary circuit model*: the model selected for the turbine describes a simplified steam turbine unit, in which a fraction of the available enthalpy drop is assumed to be converted by the High Pressure (HP) stage, whereas the remaining part to be converted by the Low Pressure (LP) one, with different time constants. The steam mass flow rate is considered proportional to the inlet pressure and governed by operating on the turbine valve admission (kv), not by throttling.

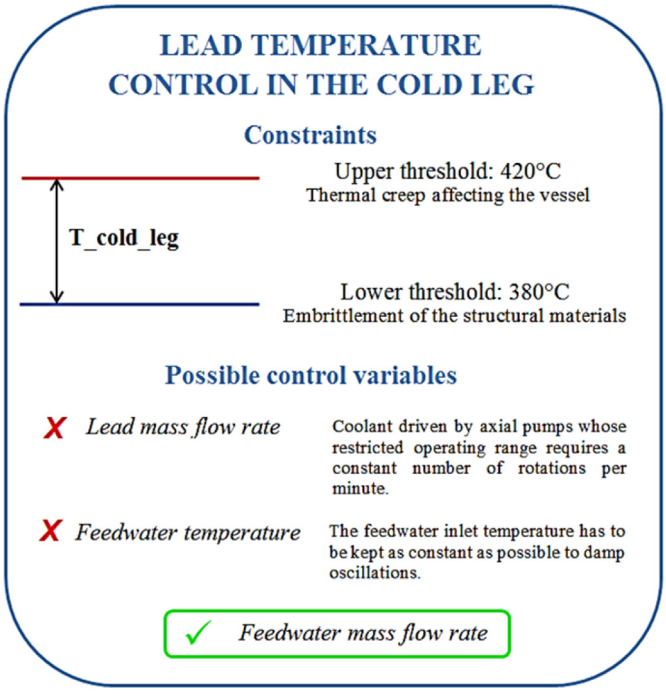

Fig. 4. Scheme indicating the concerns related to the lead temperature control in the cold leg.

As for the boundary conditions for the system modelling, the influence and the feedback on the SG due to the presence of the grid have not been allowed for. Since in this work the issues concerning the load-frequency regulation have not been studied, the grid is supposed to accept all the mechanical power produced by the NPP (i.e., the plant is operating in the "reactor leading" mode).

3.1. Design of feedback control loops

The procedure adopted for the design of the regulators is based on the use of the analysis tools of Linear Time-Invariant systems. Moreover, the same analytical approach has been employed to evaluate the level of decoupling between the different control loops. In this perspective, the previously mentioned object-oriented model has been linearized close to the nominal power conditions by means of a dedicated feature of the Dymola simulation environment. As a result of this operation, the resulting model has been expressed by adopting the following matrix-based form:

$$\begin{cases} \delta\dot{x}(t) = A\delta x(t) + B\delta u(t) \\ \delta y(t) = C\delta x(t) + D\delta u(t) \end{cases} \quad (1)$$

where A, B, C and D are the state, the input, the output, and the feedthrough matrices of the linearized system, respectively, while δu, δx and δy are the state, the output, and the input variable vectors, respectively.

As for the linearization and the subsequent order reduction of the derived system, the procedure employed and described in Ponciroli et al. (2014b) has been followed. At this point, by referring to the pairings reported in Table 2, the RGA-based analysis has been carried out so as to preliminarily evaluate the relevance of the undesired mutual influences between the selected control loops. Some details on the RGA approach adopted for this purpose are given in the Appendix. In particular, observing the RGA results in Table 3, it can be inferred that the *h_CR/Th_power*, *kv/Pressure* and *G_att/T_steam* control loops are not significantly affected by the influences due to control actions performed on other loops. On the other hand, the loop devoted to control the lead temperature in the cold leg (*T_cold_leg*) shows non-negligible interactions with other inputs. In this case, the dependence on *h_CR* via the thermal power produced has been exploited in the feedforward scheme, while the disturbances produced by the *G_att* and *kv* on *T_cold_leg* must be evaluated in order to assess that they do not constitute a concern for the regulation of this controlled variable.

If the interactions are negligible, the overall system can be studied as a set of SISO control loops independent of each other. This assumption, which will be proved in Section 4, permits studying separately the different control loops, without allowing for the inevitable interactions among them. Consequently, the parameters of the implemented PI regulators can be calibrated by adopting the procedures commonly employed for the SISO systems. In particular, for each control loop, the tuning has been performed

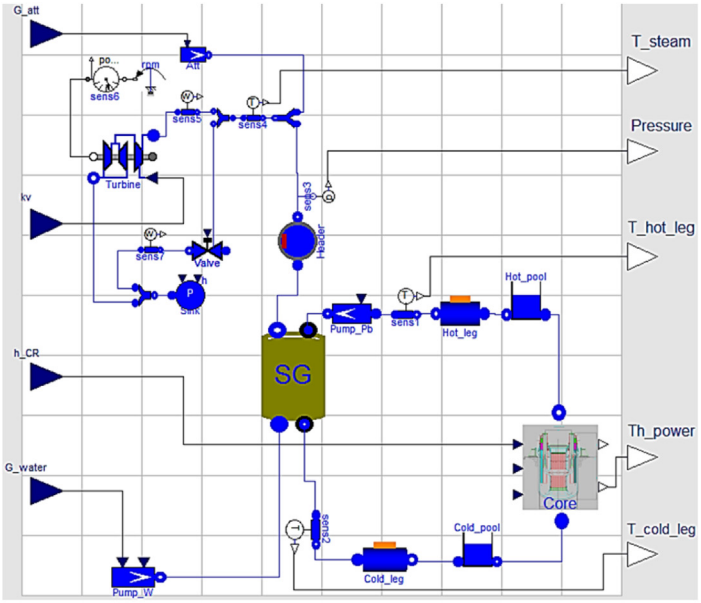

Input variables	Definition
G_att	Attemperator mass flow rate
kv	Turbine admission valve coefficient
h_CR	Control rod height
G_water	Feedwater mass flow rate

Output variables	Definition
T_steam	Turbine inlet steam temperature
Pressure	SG pressure
T_hot_leg	Temperature of lead flowing out the core
Th_power	Thermal power produced within the core
T_cold_leg	Temperature of lead flowing into the core

Fig. 5. Object-oriented model of the ALFRED reactor. In particular, it possible to observe the input/output variables employed in the control scheme developed in the present work.

Table 2
Selected pairings for the full power mode operation.

Control variable	Controlled variable	Controller
Control rods height (*h_CR*)	Thermal power (*Th_power*)	Feedback
Turbine admission valve (*kv*)	SG Pressure (*Pressure*)	Feedback
Attemperator mass flow rate (*G_att*)	Turbine inlet temperature (*T_steam*)	Feedback
Feedwater mass flow rate (*G_water*)	Cold leg lead temperature (*T_cold_leg*)	Feedback + Feedforward

Table 3
Interaction level evaluation performed by means of the RGA method. The red values represent the elements that correspond to the selected input/output pairings.

OUTPUTS	INPUTS			
	h_CR	***G_water***	***kv***	***G_att***
T_cold_leg	0.3565	**0.3571**	-0.0401	0.3265
T_steam	0.0002	-0.0002	0.0778	**0.9221**
Pressure	0.0000	0.4456	**0.8045**	-0.2501
Th_power	**0.6433**	0.1975	0.1578	0.0014

by adopting the Bode criterion (Levine, 1996). Generally, it is necessary to trace the Nyquist diagram of the loop function L(s)[2] to verify the asymptotic stability of the feedback system (Fig. 6). On the other hand, when L(s) does not have positive real part poles, the condition expressed by the Nyquist criterion can be verified taking advantage of the analysis of the Bode diagrams.

After having verified the applicability of the Bode criterion for each control loop, the controller parameters (i.e., the integral and the proportional ones, K_p and K_i) have been tuned so as to ensure the asymptotic stability of the individual loops (Åstrom and Hagglund, 1995). The values of these parameters are reported in Table 4. Since the controller properties in terms of phase and gain margin have been evaluated from the transfer functions of the linearized model around the nominal operating conditions, the control actions are optimized for the full power mode. Consequently, the controller performance may get worse when the system operates at conditions different from the nominal ones. It is necessary to assess the stability of the feedback system even at perturbed conditions, when the loop function is affected by uncertainties. Suitable robustness indicators allow evaluating the amplitude of the maximum disturbance on the system model so

[2] The loop function L(s) is defined as the product of the transfer function describing the process to be controlled and the transfer function corresponding to the adopted regulator, and represents the features of the feedback system.

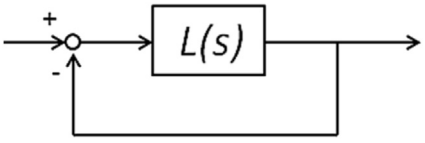

Fig. 6. Feedback scheme considered in the control scheme development.

that the stability is preserved. To this aim, thanks to the suitable values set for the corresponding parameters, it is possible to provide the regulators with a relevant phase margin. In this way, the overall control scheme will manage to effectively damp disturbances due to the change of the operating conditions, and the feedback system will be asymptotically stable even against parameter uncertainties (Franklin et al., 2014).

In NPPs, manual control is usually adopted while the plant is shut-down and during start-up to bring the plant to 40% power level, after which automatic control starts operating. Thanks to the chosen tuning that ensures a relevant phase margin, the system can be properly controlled from 40% to nominal power by means of the same controllers, and there is no need of tuning again the employed PI during the automatic full-power mode operation (i.e., updating the values chosen for K_p and K_i).

3.2. Feedforward control action

The proposed feedback scheme has been improved by adding a feedforward control action, thanks to which the water mass flow rate is adjusted according to the value of the thermal power exchanged at the SG interface. In order to point out the importance of this control action, it is worth considering the scheme in which only PI regulators are employed. In this case, when the thermal power produced in the core increases, a lead flow rate at higher temperature (i.e., *T_hot_leg* increasing) would flow to the SG. When the hotter lead reaches the SG inlet, the heat exchange conditions are not updated to the new level of thermal power to be disposed. Accordingly, the cold leg temperature tends to rise up, and only then the PI controller increases the water mass flow rate, adjusting the heat exchange conditions. Therefore, as long as the hotter lead has not passed through the SG and the lead temperature in the cold leg has not risen up, the PI controller does not perform any control action. This is not an effective strategy, since the control action is carried out too late.

On the other hand, by adopting the feedforward scheme, as soon as the lead flows into the hot leg, the value of the water flow is adjusted, and suitable cooling conditions are set before hotter lead flows at the SG inlet. Moreover, the proposed combined scheme ensures a more limited use of the PI controller and a non-negligible improvement of the phase margin as well. Indeed, a feedforward scheme is often adopted in a NPP in order to correct the output for large variations. The expression of the feedforward control action can be obtained from the following equation:

$$\Delta h^{ref} \cdot G\_water = \left(T\_hot\_leg - T\_cold\_leg^{ref}\right) \cdot c_p \cdot \Gamma_{Pb} \quad (2)$$

where Δh^{ref} is the reference value for the enthalpy drop along the SG, $T\_cold\_leg^{ref}$ is the reference value for the lead temperature in the cold leg, Γ_{Pb} is the lead mass flow rate, and c_p is the specific heat of the coolant. It is worthwhile observing that the SG heat exchange conditions are not updated according to the variation of the thermal power produced in the reactor core. Indeed, the value of the water mass flow rate that allows governing the lead temperature in the cold leg has been derived from the measurement carried out on *T_hot_leg* (Fig. 7). Otherwise, there would be the risk of producing an overcooling of the lead mass flow rate with consequent increase of reactivity and concerning power oscillations. In addition, by adopting the measurement carried out on the lead temperature, the robustness of the control system against errors on the evaluation of the time delay between the SG and the core due to transport phenomena is enhanced.

4. Interactions between control loops in the decentralized scheme

The choice of a decentralized control scheme for ALFRED reactor is based on the hypothesis that the system can be regarded as a set of uncoupled SISO control loops. This assumption can be proved by demonstrating that the interactions between the multiple-loop PI controllers are negligible or they can be filtered by the system itself. In particular, the RGA outcomes (Table 3) have pointed out that the *T_cold_leg* output may be affected by not negligible interferences (i.e., the corresponding output line shows high figures).

Once defined the *G_water/T_cold_leg* control loop, the influences of the other inputs on *T_cold_leg* have been regarded as interferences affecting the value of the controlled variable. To evaluate the incidence of these effects, the principle of superposition has been adopted, assuming that the disturbances overlap the undisturbed value of the output variable. In this perspective, dedicated transfer functions, which allow for the interactions between the control loops and evaluate the damping effect ensured by the controllers, have been introduced. In Fig. 8, a representation of two control loops is provided, with the disturbance performed by the control variable of the first loop on the controlled variable of the second loop, i.e., the *T_cold_leg*.

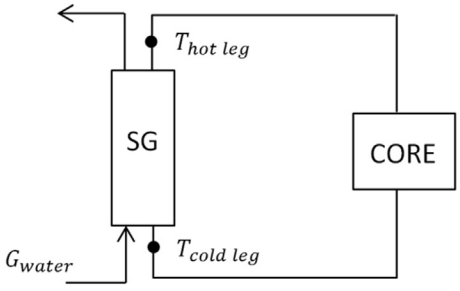

Fig. 7. Schematic view of the plant.

Table 4
Parameters of the PI controllers.

Control loop		Controller parameters		Controller performance	
Controlled variable	Control variable	K_p	K_i	Phase margin [°]	Cut-off frequency [rad s^{-1}]
T_cold_leg [°C]	G_water [kg s^{-1}]	$-6 \cdot 10^{-1}$	$-5 \cdot 10^{-4}$	99	$3.37 \cdot 10^{-3}$
Th_power [W]	h_CR [cm]	$-4 \cdot 10^{-11}$	$-1 \cdot 10^{-13}$	110	$3.32 \cdot 10^{-3}$
Pressure [Pa]	kv [-]	$-3 \cdot 10^{-7}$	$-1 \cdot 10^{-8}$	104	0.542
T_steam [°C]	G_att [kg s^{-1}]	−0.1	$-5 \cdot 10^{-2}$	93	0.083

Referring to the represented scheme, the impact of these interferences can be evaluated as follows. Denoted by $H_{12}(s)$, the "cross" transfer function is defined as:

$$H_{12}(s) = \frac{d_1(s)}{u_1(s)} \tag{3}$$

The sensitivity function $S_2(s)$ constitutes the transfer function between the noise d_1 and the output y_2, besides representing the transfer function between the set-point y_2^{ref} and the error e_2.

$$S_2(s) = \frac{1}{1 + R_2(s)G_2(s)} = \frac{1}{1 + L_2(s)} = \frac{e_2(s)}{y_2^{ref}(s)} = \frac{y_2(s)}{d_1(s)} \tag{4}$$

In particular, it accounts for the filtering action performed by the dedicated control loop, represented by $L_2(s) = R_2(s) \cdot G_2(s)$. Under the hypothesis of asymptotic stability, the feedback control loop performs a damping effect on the noise components at lower pulsation than the cut-off frequency, ω_c.

Another relevant transfer function is the complementary sensitivity function $F_1(s)$, defined as:

$$F_1(s) = \frac{R_1(s)G_1(s)}{1 + R_1(s)G_1(s)} = \frac{L_1(s)}{1 + L_1(s)} = \frac{y_1(s)}{y_1^{ref}(s)} \tag{5}$$

which represents the transfer function between the set-point and the corresponding controlled variable. Finally, the relationship between the reference signal input for the controlled variable 1 (i.e., y_1^{ref}) and the resulting control action determined by the regulator (i.e., u_1) has been considered. Dividing $F_1(s)$ by the transfer function that describes the characteristic process of the loop 1, $G_1(s)$, the transfer function between the set-point of the control loop 1 and the corresponding input variable is obtained:

$$\frac{F_1(s)}{G_1(s)} = \frac{L_1(s)}{1 + L_1(s)} \cdot \frac{1}{G_1(s)} = \frac{R_1(s)}{1 + L_1(s)} = \frac{y_1(s)}{y_1^{ref}(s)} \cdot \frac{u_1(s)}{y_1(s)} = \frac{u_1(s)}{y_1^{ref}(s)} \tag{6}$$

Multiplying this expression by the "cross" transfer function, $H_{12}(s)$, and weighting the result for the sensitivity function of the control loop 2, $S_2(s)$, the overall transfer function $A(s)$ is achieved:

$$A(s) = \frac{R_1(s)}{1 + L_1(s)} \cdot H_{21}(s) \cdot S_2(s) = \frac{u_1(s)}{y_1^{ref}(s)} \cdot \frac{d_1(s)}{u_1(s)} \cdot \frac{y_2(s)}{d_1(s)} = \frac{y_2(s)}{y_1^{ref}(s)} \tag{7}$$

The transfer function $A(s)$ represents the influence of y_1^{ref} on y_2 whether the influence performed by u_2 on y_1 is not taken into account. Indeed, the disturbance produced by the first loop on the second one is caused in part by the control variable u_1 and in part by the interference due to the second loop, and the latter plays through the first loop an interference on the variable of interest y_2. Nevertheless, this additional noise is secondary since its effect is filtered twice both by the transfer functions of the first and second loop, before producing an effect on y_2. Therefore, the approximation of neglecting this contribution can be adopted for our purposes and $A(s)$ represents the transfer function between y_1^{ref} and y_2.

In particular, the maximum value assumed by $|A(j\omega)|$ over the pulsation range of interest represents the numerical factor for which the value of the set-point for the control loop 1, y_1^{ref}, must be multiplied in order to get the maximum possible disturbance performed on the controlled variable of the control loop 2, y_2, net of the filtering actions performed by the involved control loops.

At this point, the transfer functions related to *T_cold_leg*, such as *kv/T_cold_leg* and G_{att}/*T_cold_leg*, have been considered in order to evaluate the impact of the two disturbances on the controlled variable y_2 (i.e., *T_cold_leg*).

For the sake of completeness, on the basis of this inequality, the upper bounds of the performed disturbances have been estimated for all the implemented control loops (Table 5). The Bode diagrams of the transfer function $A(s)$ adopted in this analysis have been reported in Fig. 9. A simplified model has been implemented in SIMULINK® (MATLAB® and SIMULINK® software, 2005) so as to compare the analytical analysis with numerical simulations (Fig. 10). In Fig. 11, the behaviour of the lead temperature following the previously mentioned input variations is shown, and the maximum elongations during the transient turn out to be coherent with the foreseen upper bound, assessing the initial hypothesis of neglecting the interferences between the selected control loops.

5. Control rod actuator

In the finalization of the control scheme, after having selected the most effective pairings between the input and output variables and assessed the level of decoupling of the control loops, the design of the actuators is carried out. In control systems, limiters are usually set on the rate of variation of the performed control actions, so as to avoid jeopardizing the integrity of the components. This aspect assumes a dramatic relevance in NPPs as far as the externally-imposed reactivity is concerned (Bernard, 1999). During any power transient, prompt criticality condition must be avoided, otherwise the multiplying system turns out to be critical without the contribution of delayed neutrons, and the power increase cannot be longer controlled by operating the control rods. Since the system reactivity cannot be directly measured, most of the operational procedures do not refer to it. Instead, a dedicated constraint is specified on the value assumed by the reactor period, τ, which is defined as:

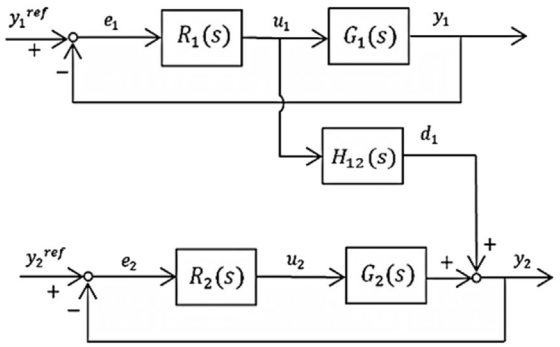

$R(s)$	Controller transfer function
$G(s)$	Controlled process transfer function
$H(s)$	Cross transfer function
y^{ref}	Set-point of the control loop
y	Controlled variable
e	Error between y^{ref} and y
u	Control variable
d	Disturbances

Fig. 8. SISO control loops and representation of the mutual interactions.

Table 5
Upper bounds of the disturbances performed by the different control loops on each other.

Input variation	Controlled variables variation			
	δTh_power [MW]	δT_cold_leg [°C]	$\delta Pressure$ [bar]	δT_steam [°C]
1 MW on Th_power^{ref}	–	0.1827	$1.11 \cdot 10^{-3}$	0.0172
1 °C on $T\_cold\_leg^{ref}$	0.4803	–	0.2259	0.6679
1 bar on $Pressure^{ref}$	0.1603	0.1528	–	0.6157
1 °C on T_steam^{ref}	0.07609	0.0715	$6.912 \cdot 10^{-5}$	–

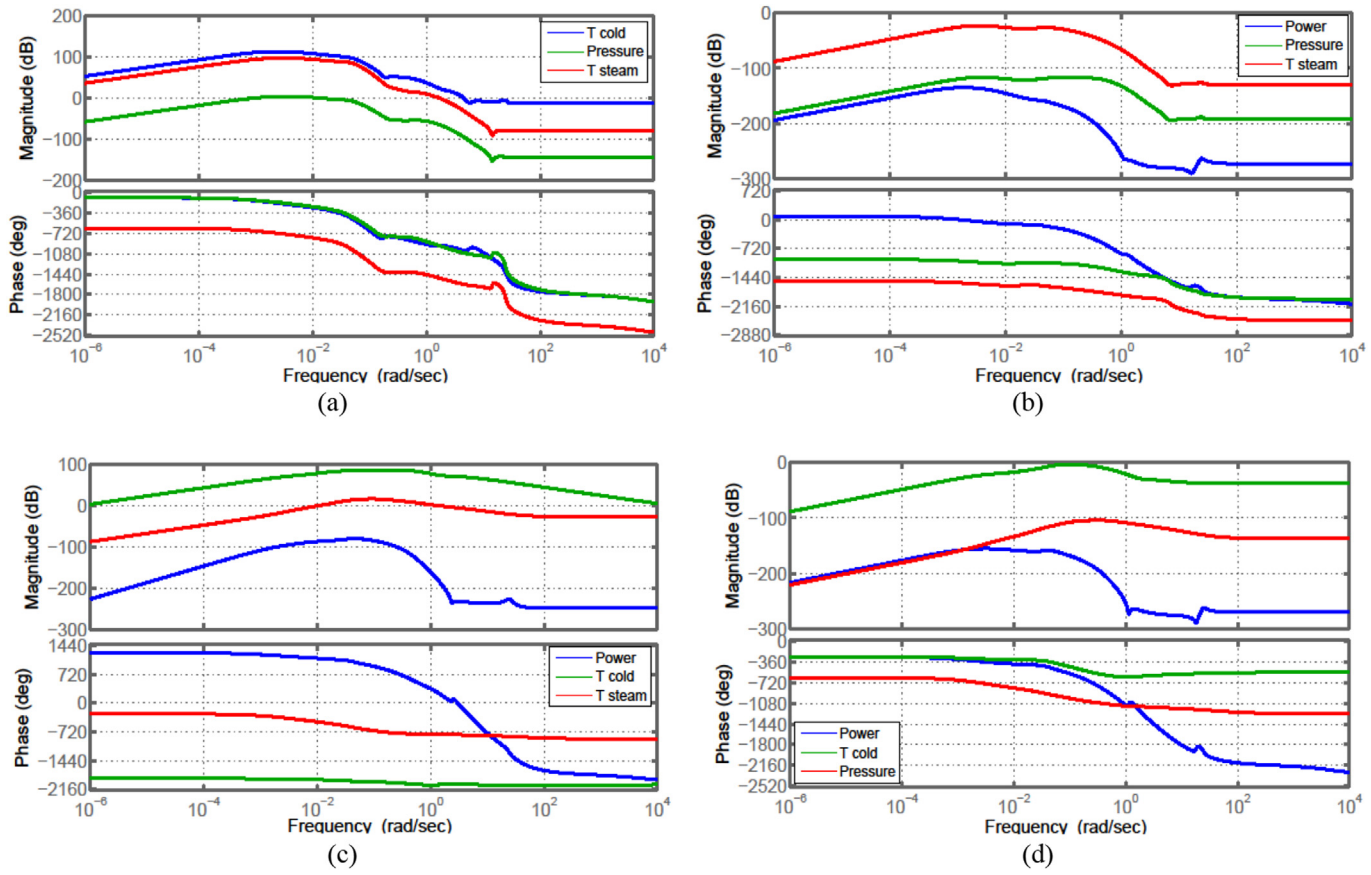

Fig. 9. Representation of the several transfer functions which allow to evaluate the interactions between the different control loops: (a) A(s) transfer functions, which represent the impact of $T\_cold\_leg^{ref}$, $Pressure^{ref}$ and T_steam^{ref} on the output Power; (b) A(s) transfer functions, which represent the impact of Th_Power^{ref}, $Pressure^{ref}$ and T_steam^{ref} on the output T_cold_leg; (c) A(s) transfer functions, which represent the impact of Th_Power^{ref}, $T\_cold\_leg^{ref}$, T_steam^{ref} on the output Pressure; and (d) A(s) transfer functions, which represent the impact of Th_Power^{ref}, $T\_cold\_leg^{ref}$, $Pressure^{ref}$ on the output T_steam.

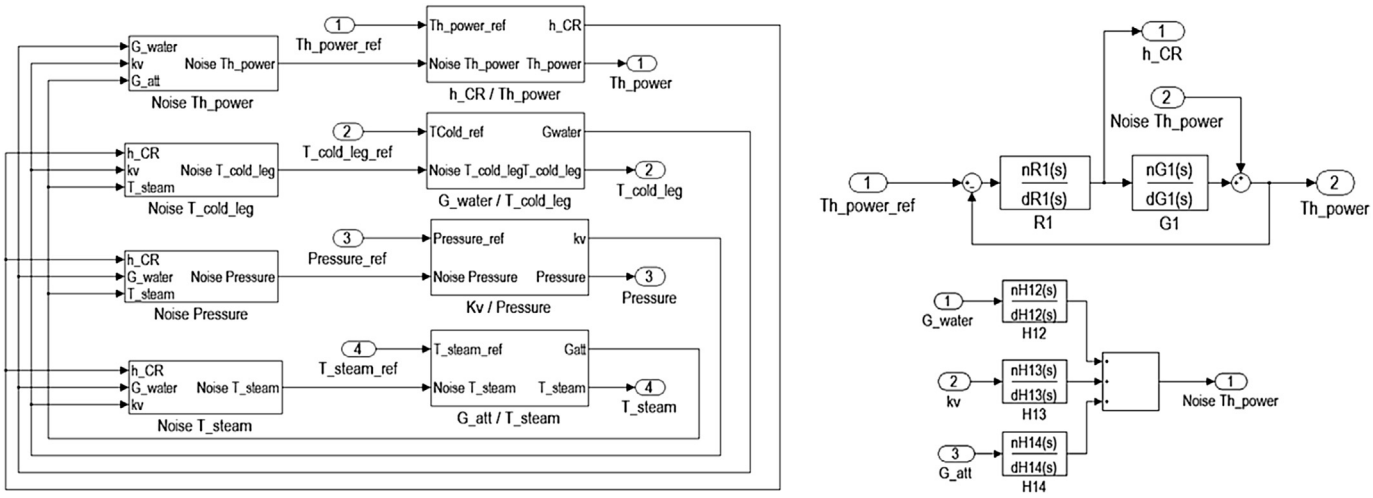

Fig. 10. Block scheme employed to evaluate the mutual influences of the different control loops on each other.

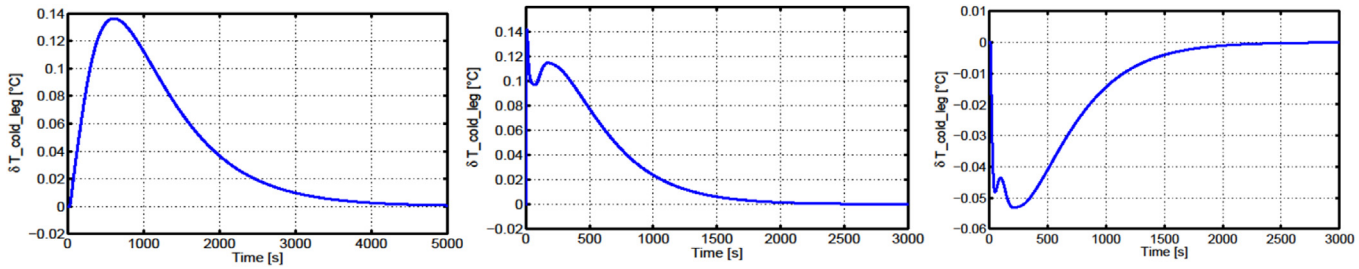

Fig. 11. Effects on the T_cold_leg due to the different control actions performed by changing the set-point of the other controlled variables: (a) T_cold_leg behaviour during a transient produced by a 1 MW variation imposed on Th_power^{ref}; (b) T_cold_leg behaviour during a transient produced by a 1 bar variation imposed on Pressure^{ref}; and (c) T_cold_leg behaviour during a transient produced by a 1 °C variation imposed on T_steam^{ref}.

$$\tau = \frac{n(t)}{dn/dt} \tag{8}$$

where n(t) is the neutron population. The reactor period must be large enough to allow performing control actions on the system. If its value drops below a certain threshold, the power level increases so fast that the actuators are not able to govern the system evolution. This aspect must be taken into account in the design of the dedicated controller by imposing an upper limit to the maximum extraction speed of the CRs. To this aim, and given that for LFRs no operational experience is available, a methodology to define a threshold value for the CRs extraction speed has been proposed. Based on the outcomes of the linear stability analysis of the ALFRED reactor, the Bode diagram of the transfer function between the externally-imposed reactivity and the system reactivity feedback is obtained. Starting from this transfer function, a suitable criterion has been derived.

In Fig. 12, the Bode diagrams of the transfer function between the reactivity governed by extracting CRs (ρ_{rods}) and the system thermal reactivity feedbacks (ρ_{temp}), evaluated at different power levels (from 10% to nominal conditions), are represented. In particular, considering Bode diagrams for the module, these curves can be approximated by a first-order transfer function (Åstrom and Hagglund, 1995) as follows:

$$G(s) = \frac{\rho_{temp}}{\rho_{rods}} = -\frac{1}{1 + s\tau_{temp}} \quad \tau_{temp} = \frac{1}{\omega_{temp}} \tag{9}$$

where τ_{temp} is the reciprocal of the characteristic angular frequency (ω_{temp}) at which the Bode diagram undergoes a rapid change of slope. As for the reactivity insertion, it has been modelled as it would take place in a continuous way as a ramp. The slope of this ramp has been parameterized, imposing that the time necessary to the CRs to insert a reactivity equal to one dollar (i.e., τ_{rise}) allows the reactivity feedbacks to restore critical equilibrium conditions:

$$\frac{d\rho_{rods}}{dt} = \frac{\beta}{\tau_{rise}} \Rightarrow \rho_{rods}(s) = \frac{\beta}{s^2\tau_{rise}} \tag{10}$$

where β is the fraction of the delayed neutrons. At this point, it is necessary to find out an expression that allows associating the state variable ρ_{rods} to the CRs extraction speed. The curve of integral reactivity features a sinusoidal dependence of the CRs position, as shown in Fig. 13.

Therefore, the positive reactivity insertion rate can be expressed as function of the CRs extraction speed, v_{ext}, as follows:

$$\frac{d\rho_{rods}}{dt} = \frac{d}{dt}\left[\left(\frac{\partial\rho_{rods}}{\partial x}\right)\cdot dx\right] = \left(\frac{\partial\rho_{rods}}{\partial x}\right)\cdot v_{ext} \tag{11}$$

Inserting Eq. (11) in Eq. (10), it is obtained:

$$v_{ext}(x) = \left(\frac{\beta}{\tau_{rise}}\right)\cdot\left(\frac{1}{\partial\rho_{rods}/\partial x}\right) \tag{12}$$

It can be noticed that the CRs extraction speed depends on the position at which they are located within the core, since their effectiveness $\rho_{rods}(x)$ depends on the position. The reactivity contribution due to thermal feedbacks in response to a control rod insertion, ρ_{temp}, is given by:

$$\rho_{temp}(s) = G(s)\cdot\rho_{rods}(s) = -\frac{1}{1 + s\tau_{temp}}\cdot\frac{\beta}{s^2\tau_{rise}} \tag{13}$$

This expression has been decomposed by means of the Heaviside method (Ogata, 2009):

$$\rho_{temp}(s) = -\frac{\beta\tau_{temp}^2/\tau_{rise}}{1 + s\tau_{temp}} + \frac{\tau_{temp}}{\tau_{rise}}\cdot\frac{\beta}{s} - \frac{\beta}{\tau_{rise}}\frac{1}{s^2} \tag{14}$$

By calculating the inverse transform of Eq. (14), the reactivity due to the thermal feedbacks is obtained:

$$\rho_{temp}(t) = \left[\beta\frac{\tau_{temp}}{\tau_{rise}}\left(1 - e^{-t/\tau_{temp}}\right)H(t) - \frac{\beta}{\tau_{rise}}ram(t)\right] \tag{15}$$

where ram(t) and H(t) represent the unit ramp and the unit step signal provided as inputs, respectively. If the positive reactivity introduced into the system by handling CRs is added to Eq. (15), the overall system reactivity during the power transient, ρ(t), can be finally achieved:

$$\rho(t) = \rho_{rods}(t) + \rho_{temp}(t) = \beta\frac{\tau_{temp}}{\tau_{rise}}\left(1 - e^{-t/\tau_{temp}}\right)H(t) \tag{16}$$

The maximum value assumed by this function is equal to:

$$\rho(t)_{\max} = \beta\frac{\tau_{temp}}{\tau_{rise}} \tag{17}$$

In order to avoid prompt criticality condition, the system reactivity must not exceed the value of one dollar during the operational transients. Consequently, a constraint can be set by imposing that the maximum value assumed by the reactivity is less than a certain fraction of the dollar, represented by a suitable coefficient, K_{safety}:

$$\rho(t)_{\max} < K_{safety}\cdot\beta \tag{18}$$

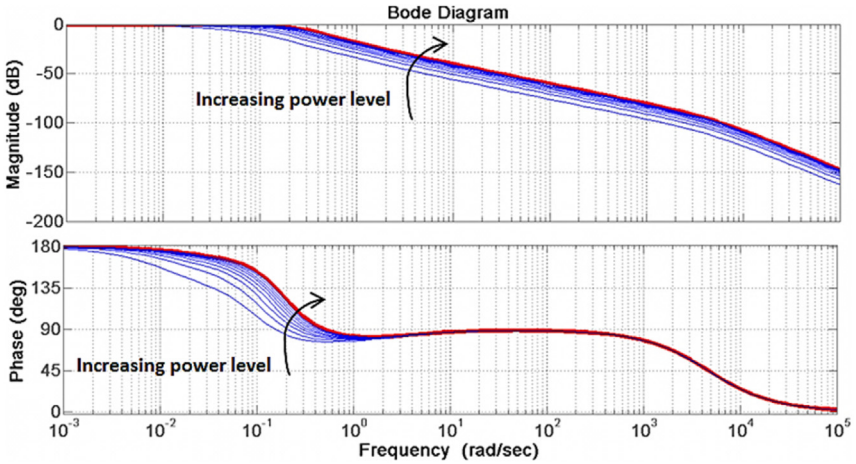

Fig. 12. Bode diagrams for the transfer function between externally-imposed reactivity and system reactivity feedback, at different power levels. In particular, the red curve is referred to the transfer function evaluated at nominal power level, while the other ones are referred to reduced power levels. (For interpretation of the references to colour in this figure legend, the reader is referred to the web version of this article.)

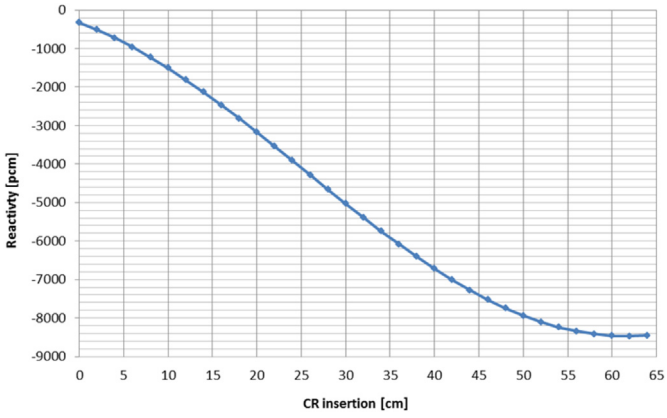

Fig. 13. Integral reactivity curve for the ALFRED control rods.

Substituting in Eq. (18) the maximum value assumed by the reactivity during the transient (Eq. (17)) and the definition of CRs extraction speed (Eq. (12)), it is obtained:

$$v_{ext}(x) \leq \frac{K_{safety} \cdot \beta}{\frac{\partial \rho_{rods}}{\partial x}(x) \cdot \tau_{temp}} \tag{19}$$

It can be noted that v_{ext} turns out to be:

- proportional to $1/\tau_{temp}$ (i.e., the faster the dynamics of reactivity feedback, the higher extraction speed of CRs can be adopted);
- proportional to β (i.e., the higher the fraction of delayed neutrons, the easier controlling the transients of the system);
- inversely proportional to $\partial\rho_{rods}/\partial x$ (i.e., the higher value of the control rods, the lower the extraction speed).

Starting from this result, a safety limit to the extraction speed of the control rods has been evaluated by adopting the system parameters reported in Table 6 and implemented in the corresponding control loop.

6. Simulation of control scheme performance

In order to assess the performance of the developed control scheme, several operational transients have been simulated (Ponciroli, 2014). In this work, two of them have been selected to be presented. The former consists in a 10% reduction of the reactor power from nominal load conditions, while the latter consists in a 10% increase of the reactor power starting from 60% load conditions. For each transient, the dynamic behaviour of the controlled variables (i.e., thermal power produced within the core, pressure in the SG, lead temperature in the cold leg, turbine inlet temperature) have been reported. In Figs. 14 and 15, the red lines represent the set-points of the controlled variables, while the blue ones are the corresponding trajectories.

6.1. 10% power level reduction starting from nominal conditions

Firstly, the control system effectiveness has been tested around the nominal operating conditions, simulating a step-wise load reduction of 30 MW. As for the thermal power control loop, the most relevant figure of merit is constituted by the settling time, which is defined as "the time required for the response curve to reach and stay within a 2% of the final value" (Ogata, 2009). In the simulated operational transient, its value is about 700 s and the definitive equilibrium condition is reached in 1000 s, as shown in Fig. 14a. The relevant slowness of the dynamic response is partially due to the choice of reducing the control system performance in order to ensure control system robustness, but it is mainly a inherent feature of LFRs. As it has been observed in the free dynamics simulations (Ponciroli et al., 2014a), the characteristic large thermal inertia due to the pool and the transport phenomena along hot and cold collectors inevitably influence the controlled system response. On the other hand, as for the other control loops, the pressure in the SG reaches a maximum elongation of 0.15 bar, while the steam temperature at the turbine inlet never deviates by more than 0.2 °C from its nominal value, as shown in Fig. 14b–c. Finally,

Table 6
Parameters used to evaluate the maximum CRs extraction speed.

Parameter	Value
K_{safety}	0.4
β	334.6 pcm
τ_{temp}	10 s
$d\rho_{rods}/dx$	132.813 pcm cm^{-1}
v_{ext}	0.126 cm s^{-1}

the evolution of the lead temperature at the SG outlet (Fig. 14d) confirms the effectiveness of the proposed control scheme. Indeed, the disturbances are effectively damped (the value of the controlled variable never deviates more than 0.25 °C from the set-point).

6.2. 10% power level increase starting from 60% load conditions

Secondly, a demanding operational transient has been simulated in order to test the performance of the proposed control scheme at quite different conditions from the nominal ones as well. After having achieved 60% load conditions, the system has been stabilized, and then a 10% power increase has been simulated.

As it can be seen in Fig. 15a, the control loop dedicated to govern the thermal power produced in the reactor core shows satisfying performance even at 60% load factor, since the power transient can be considered concluded within 1000 s. It is then relevant to consider the lead temperature in cold leg control loop (Fig. 15b). Even after a 40% load transient, the adopted control scheme manages preventing the temperature of the lead to deviate by more than 1 °C from the reference value.

The most challenging aspect concerns the steam temperature at the turbine inlet, as shown in Fig. 15c. Indeed, since the lead temperature control in the cold leg is performed by operating on the feedwater mass flow rate in the secondary circuit, this control variable hardly can meet the BoP demands. In nominal conditions, a minimum flow of water is introduced into the superheated steam, but during this very demanding transient at reduced load conditions the steam temperature cannot be finely adjusted. Finally, SG pressure control loop (Fig. 15d) has demonstrated very satisfactory performance, even after a step change in the power and then after a rather abrupt variation of the water mass flow rate. Indeed, the pressure never deviates for more than 0.5 bar of the set-point, thus avoiding relevant mechanical stress to the SG.

7. Conclusions

In the present work, the assessment of the control system for the full power mode operation of the ALFRED reactor, based on the classical approach of feedforward-feedback controllers, has been presented. In preliminary investigations (Ponciroli et al., 2014a, 2014b), starting from the results of the free dynamics simulation confirmed by the RGA method, different control strategies have been considered. In this paper, the finalization of the control scheme for the ALFRED full-power mode has been performed by taking into account the design choices made for this reactor. Indeed, in order to limit the feedwater inlet temperature variations, a dedicated device has been envisaged in the BoP, whereas the value of the lead mass flow rate has to be maintained constant because of the features of the pumps employed in the primary circuit. Therefore, once having selected the pairings between input and output variables, the corresponding transfer functions have been derived from the linearized system so as to evaluate the impact of the mutual influences among the identified control loops. In particular, it has been possible to damp the interferences, demonstrating the feasibility of the proposed decentralized control scheme. The results of the simulated operational transients have shown the effectiveness of the developed linear control system, whose controller parameters have been tuned in order to provide a compromise among performance, robustness and safety margins. As for the actuators design, instead of adopting an empirical approach to define the maximum extraction speed of the control rods, it has been decided to derive its operational value starting from the previously performed stability analysis. In this way, a procedure for this innovative reactor concept, for which no operational experience is available, has been defined.

To conclude, in this work, a suitable control strategy for the ALFRED reactor has been ascertained. It allows adjusting the thermal power production in the core and the SG operation, ensuring

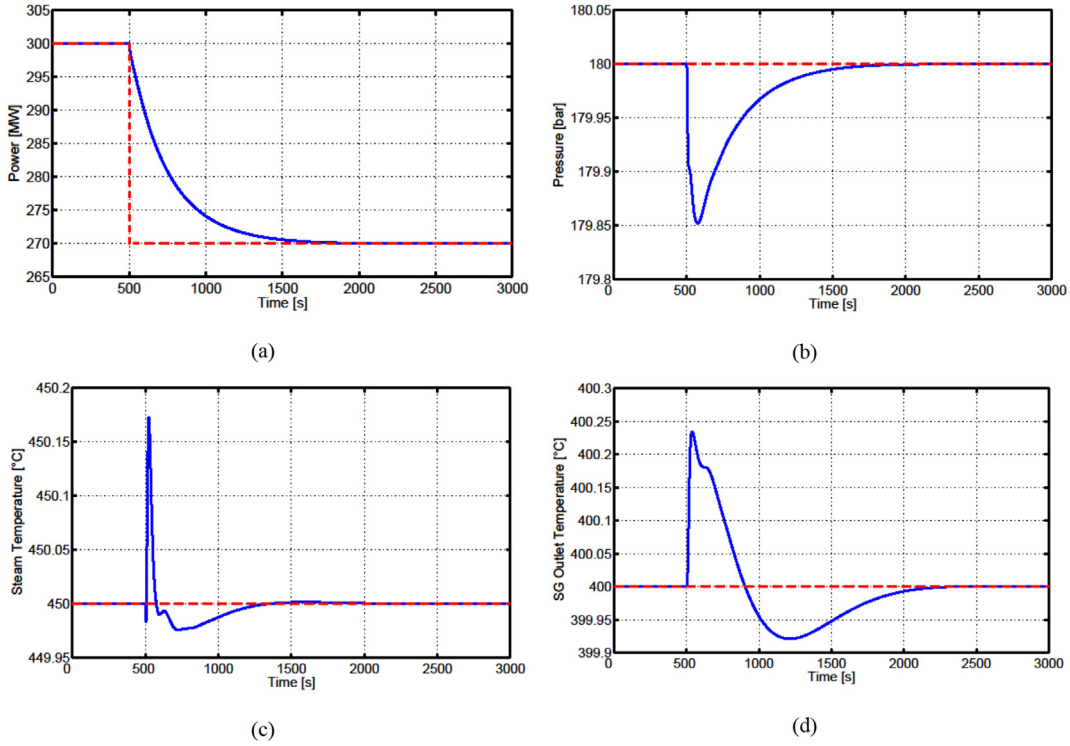

Fig. 14. Controlled responses of the different output variables after a 10% power level reduction starting from nominal conditions: (a) reactor power evolution; (b) SG pressure evolution; (c) steam temperature evolution; and (d) lead temperature in the cold leg evolution.

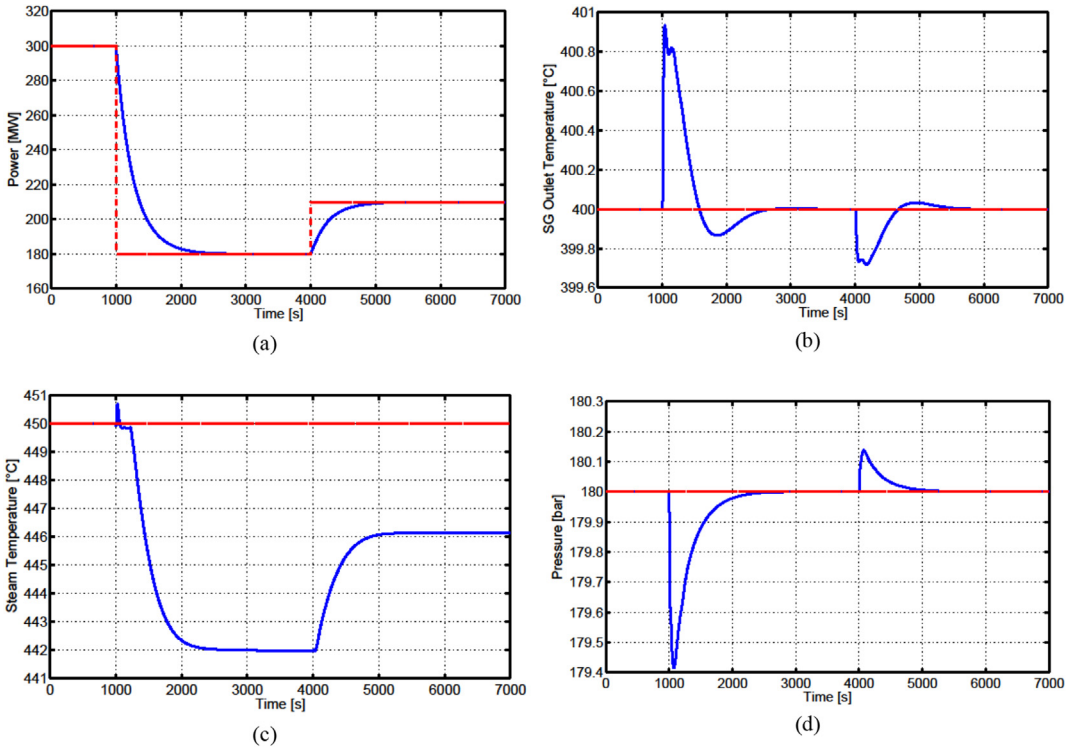

Fig. 15. Controlled responses of the different output variables after a 10% power level increase starting from 60% load conditions: (a) reactor power evolution; (b) SG pressure evolution; (c) steam temperature evolution; and (d) lead temperature in the cold leg evolution.

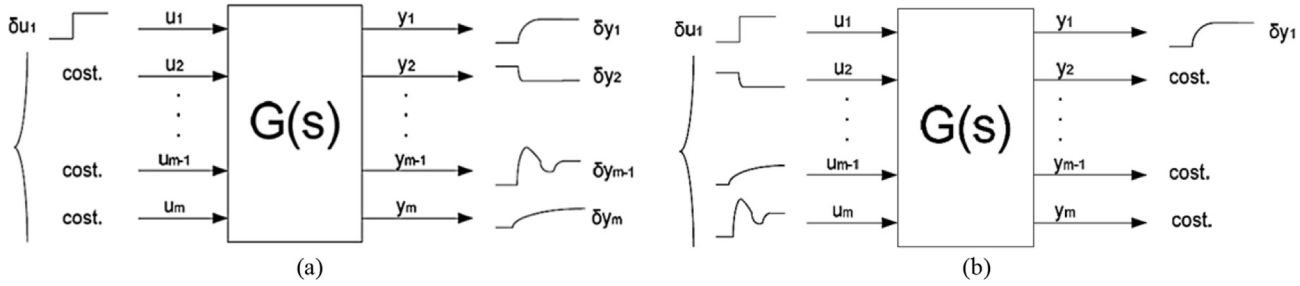

Fig. 16. Representation of an open loop response (a), and of a closed loop response (b). In particular, the physical process to be controlled (G(s)), the system output variables (y_j), the corresponding variation (δy_j), the system input variables (u_i), and the corresponding variation (δu_i) are shown.

the lead in the cold pool to remain in a safe temperature range. As for the further developments, the aspects concerning the load-frequency regulation are investigated in a parallel work (Ponciroli et al., 2015). Indeed, though in the present paper the "reactor leading" mode has been assumed, it is necessary to evaluate the influence on the SG due to the mechanical power modulation in accordance with the load demands, and how the issue of the slow system dynamics can be overcome in the light of the performance required by the grid.

Acknowledgements

The authors acknowledge the European Commission for funding the LEADER Project in its 7th Framework Programme. Acknowledgment is also due to all the colleagues of the participant organizations for their contributions in many topics, in particular to Dr. Alessandro Alemberti and Dr. Luigi Mansani (Ansaldo Nucleare) for their valuable support and fruitful criticism.

Appendix. Relative gain array approach

In the design of a decentralized control scheme, the first step to be taken is constituted by the selection of the most effective pairings between control and controlled variables. Accordingly, the input showing the most relevant interaction with a certain output, and at the same time not significantly affecting the evolution of the other variables of interest, represents the ideal candidate. Interactions among variables constitute a physical feature of the system, and the best hints for the pairing can be derived by analysing the free dynamics response of the plant. These indications can be supported by some dedicated techniques, such as the RGA method. This procedure is a heuristic method that allows determining the most effective input to control each variable of interest, providing useful suggestions on how the model-based decentralized control system should be structured.

The effectiveness of a feedback control loop can be assessed by characterizing the MIMO (*Multiple Inputs and Multiple Outputs*)

system behaviour both in *open loop* and *closed loop* conditions. As for the open loop gain, considering the system at equilibrium condition for fixed constant values of control variables, a step variation of amplitude δu_i on a certain input u_i is performed, causing a variation of the quantity δy_{jOL} of each output variable y_j (Fig. 16a). The open loop gain is defined as

$$g_{ji} = G_{ji}(0) = \frac{\delta y_{jOL}}{\delta u_i} \tag{20}$$

where $G_{ji}(0)$ is regarded as the gain of the transfer function between u_i and y_j. Instead, for the closed loop gain, it is assumed that, against the same variation of δu_i, an action is performed on all the other input variables in order to keep all the other outputs fixed, except for y_j, thanks to the action carried out by the other inputs (Fig. 16b). If the variation of y_j in closed loop configuration is indicated with δy_{jCL}, the closed loop gain between u_i and y_j can be defined as

$$h_{ji} = \frac{\delta y_{jCL}}{\delta u_i} \tag{21}$$

If the static gain for the open loop (g_{ji}) and for the closed loop (h_{ji}) are evaluated for all the input–output pairs, the RGA matrix Λ can be obtained. This matrix can be regarded as a quantitative measure of the input–output interaction at zero frequency for asymptotically stable processes. In particular, the elements λ_{ji} of this matrix, namely the relative gain of the pair (u_i, y_j), are defined as:

$$\lambda_{ji} = \frac{g_{ji}}{h_{ji}} \tag{22}$$

In a control system development perspective, when the value of a λ_{ji} element approaches unity, there is a fair interaction that can be exploited, whereas if the value of a λ_{ji} element approaches zero the involved variables can be regarded as uncoupled. If the matrix element λ_{ji} is negative, it means that the control action may produce effects opposite to the desired ones on the controlled variable, depending on whether feedback control loops involve other output variables or not (Skogestad and Postlethwaite, 2005).

References

Alemberti, A., Frogheri, M., Mansani, L., 2013. The Lead fast reactor demonstrator (ALFRED) and ELFR design. In: Proceedings of the International Conference on Fast Reactors and Related Fuel Cycles: Safe Technologies and Sustainable Scenarios (FR 13), Paris, France, March 4-7, 2013.

Åstrom, K.J., Hagglund, T., 1995. PID Controllers: Theory, Design, and Tuning. Instrument Society of America, Research Triangle Park, North Carolina.

Bernard, J.A., 1999. In: Webster, J.G. (Ed.), Light Water Reactor Control Systems. Wiley Encyclopedia of Electrical and Electronics Engineering, New York, NY.

Bortot, S., Cammi, A., Lorenzi, S., Ponciroli, R., Della Bona, A., Juarez, N.B., 2013. Stability analyses for the European LFR Demonstrator. Nucl. Eng. Des. 265, 1238–1245.

Bristol, E.H., 1966. On a new measure of interaction of multivariable process control. IEEE Trans. Autom. Control 11, 133–134.

DYNASIM, 2006. Dymola Version 6.1. Dynasim AB. Lund, Sweden, Homepage. http://www.dynasim.se.

Damiani, L., Montecucco, M., Pini Prato, A., 2013. Conceptual design of a bayonet-tube steam generator for the ALFRED lead-cooled reactor. Nucl. Eng. Des. 265, 154–163.

Franklin, G.F., Powell, J.D., Emami-Naeini, A., 2014. Feedback Control of Dynamic Systems. Prentice Hall.

Fritzson, P., 2004. Principles of Object-oriented Modeling and Simulation with Modelica 2.1. Wiley-IEEE Press.

GIF, 2002. A Technology Roadmap for Generation IV Nuclear Energy Systems. Technical Report GIF-002–00.

Grasso, G., Petrovich, C., Mikityuk, K., Mattioli, D., Manni, F., Gugiu, D., 2013. Demonstrating the effectiveness of the European LFR concept: the ALFRED core design. In: Proceedings of the International Conference on Fast Reactors and Related Fuel Cycles: Safe Technologies and Sustainable Scenarios (FR 13), Paris, France, March 4-7, 2013.

http://www.leader-fp7.eu/(accessed 02.07.15).

Levine, W.S., 1996. The Control Handbook. IEEE Press.

MATLAB® and SIMULINK® Software, 2005. The MathWorks, Inc.

Ogata, K., 2009. Modern Control Engineering. Prentice Hall.

Ponciroli, R., 2014. Development of a Model-based Approach for Studying the System Dynamics and Control of Gen-iv Lead-cooled Fast Reactors. Politecnico di Milano. Ph.D. Thesis.

Ponciroli, R., Bigoni, A., Cammi, A., Lorenzi, S., Luzzi, L., 2014a. Object-oriented modelling and simulation for the ALFRED dynamics. Prog. Nucl. Energy 71, 15–29.

Ponciroli, R., Cammi, A., Lorenzi, S., Luzzi, L., 2014b. A preliminary approach to the ALFRED reactor control strategy. Prog. Nucl. Energy 73, 113–128.

Ponciroli, R., Cammi, A., Lorenzi, S., Luzzi, L., 2015. Control approach to the load frequency regulation of a Generation IV Lead-cooled Fast Reactor. Energy Convers. Manage. 103, 43–56.

Skogestad, S., Postlethwaite, I., 2005. Multivariable Feedback Control: Analysis and Design. John Wiley and Sons.

Tucek, K., Carlsson, J., Wider, H., 2006. Comparison of sodium and lead-cooled fast reactors regarding reactor physics aspects, severe safety and economic issues. Nucl. Eng. Des. 236, 1589–1598.